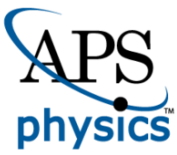

Novel mechanism for order patterning in alloys driven by irradiation

C. R. Lear, P. Bellon, and R. S. Averback

Phys. Rev. B **96**, 104108 — Published 18 September 2017

DOI: 10.1103/PhysRevB.96.104108

A novel mechanism for order patterning in alloys driven by irradiation

C. R. Lear*, P. Bellon and R.S. Averback

Department of Materials Science and Engineering, University of Illinois at Urbana-Champaign, Urbana, IL 61801, USA

** Now at Department of Nuclear Engineering and Radiological Sciences, University of Michigan, Ann Arbor, MI 48109, USA*

Abstract:

Kinetic Monte Carlo simulations have been performed to investigate the evolution of ordered domains in model alloys under irradiation. The alloys investigated were equiatomic binary alloys on a simple square lattice with first and second nearest-neighbor interactions, chosen so that a 2×2 ordered structure is the equilibrium phase below a critical order-disorder transition temperature, T_c. The ratio of second to first nearest neighbor interactions, R was varied from 0 to 0.45 to explore the effect of the thermodynamic frustrations induced by the proximity of the 2×1 phase boundary, which occurs at R = 0.5 for T = 0. The atomic mixing produced by nuclear collisions was modeled by forcing the ballistic exchange of pairs of atoms at a controlled rate, Γ_b. This disordering process competed with thermodynamic re-ordering, resulting in non-equilibrium steady states. Two trivial steady states were found, a disordered state at high Γ_b and low T, and a long-range ordered state at low Γ_b and low T. In the R=0.45 alloy, however, a third steady state was identified at intermediate Γ_b and T values, where multiple long-range ordered domains coexisted dynamically. It is shown that this state of patterning of order resulted from the coupling of the thermodynamic frustrations present in that alloy with the disorder introduced by irradiation. The practical relevance of this

novel mechanism for patterning of order under irradiation is discussed in the context of recent observations of domain co-existence in irradiated Cu_3Au.

I. Introduction

Irradiation of hard matter with energetic projectiles such as electrons, ions, and neutrons, results in the formation of point defects and the creation of structural and chemical disorder (see for instance refs. [1-3] for reviews). A fraction of the energy deposited into the system is dissipated through relaxation processes involving the thermally activated migration of point defects. Under sustained irradiation, the competition between the continuous creation of disorder and its annealing by these relaxation processes can drive the materials into non-equilibrium steady states [2]. For alloy systems with moderate, positive heats of mixing, for instance, the forced atomic replacements generated by nuclear collisions tend to homogenize the composition field, whereas thermally activated atomic diffusion driven by thermodynamics promotes phase separation. In the case of alloy systems with negative heats of mixing, the chemical disorder created by nuclear collisions now competes with the chemical ordering promoted by thermodynamics. Using mean-field kinetic models, Martin showed that by assuming the forced atomic replacements are akin to a ballistic, i.e., athermal, diffusion, these alloy systems reach steady states that are equivalent, or nearly equivalent, to equilibrium states, albeit at a higher (effective) temperature [4]. This effective temperature captures the contribution of the non-equilibrium configurational entropy introduced by the forced atomic relocations. This model is however not general, and alloys under irradiation have been found to reach steady states that have no counterpart in

their equilibrium phase diagrams. A striking example is the case of self-organization reactions, yielding steady-state microstructures with self-selected length scales, often referred to as patterning states [5]. These self-organization reactions are similar to those often observed in other dynamical, dissipative systems such as fluid flows, chemical reactions, weather systems, or alloys undergoing solidification [5]. In the case of alloy evolutions described by the composition field, a conserved order parameter, modeling and atomistic simulations indicate that a competition between dynamic processes with distinct characteristic length scales can stabilize steady-state microstructure with finite length scales. This is the case for instance during energetic, heavy ion irradiations, where large displacement cascades force the relocation of atoms with a characteristic length scale R_b, which ranges from one atomic distance to a few nanometers [1], resulting in a non-local chemical mixing [6]. For alloys that phase separate in thermodynamic equilibrium, this forced finite-range mixing competes with thermally activated decomposition, which is short range, as point defects jump from atomic sites to nearest sites. The outcome of this scale-dependent competition can be summarized in a dynamical phase diagram in the (R_b, γ_b) space, where γ_b is a relative forcing intensity, defined as the ratio of the forced jumps over the thermal jumps. Continuum models and atomistic simulations predict that when R_b exceeds a critical value R_c compositional patterns become stable for a range of forcing intensities around $\gamma_b \approx 1$ [6-9]. These predictions are in good agreement with the compositional patterning reported in several immiscible alloys subjected to ion irradiation, including several Cu-base alloys such as Cu-Ag, Cu-Co, Cu-Fe [10-13].

In the case of chemically ordered alloys it is unclear whether irradiation can induce a similar patterning of order, as can be realized by the following kinetic equation describing the evolution of the long-range order parameter *S*:

$$\frac{\partial S}{\partial t} = -M_o \frac{\partial F}{\partial S} - \Gamma_b S \qquad (1)$$

The first term on the right-hand side of Eq. (1), which captures the thermally activated part of the kinetics, is the standard "model A", for the relaxation of non-conserved order parameters [14,15]. In this term, M_o represents a thermal mobility and F the free energy of the alloy. This free energy is usually decomposed into the free energy of an alloy with a homogeneous order S, typically a non-linear function of S, and contributions proportional $|\nabla S|^2$ and possibly higher order derivatives to capture excess energy due to spatial variations of S [15]. The second term on the right-hand side of Eq. (1) captures the disordering introduced by irradiation due to forced replacements, assumed here to be ballistic events taking place at a rate Γ_b [16,17]. In this simple approach, the disordering introduced by irradiation does not introduce any new length scale, and therefore it is not expected to induce patterning of the field S. This conclusion is supported by a simple linear stability analysis of Eq. (1) [18]. That equation, however, relies on several simplifications; for instance, it does not capture the fact that energetic displacement cascades introduce chemical disorder as large disordered zones [19,20]. Kinetic Monte Carlo simulations indicated that when the re-ordering of these zones promotes the nucleation of new ordered domains a steady state comprised of multiple, co-existing ordered domains is found in a region of the (T, Γ_b) parameter space where ordering and

disordering rates are of similar magnitude [21,22]. In this patterning state the maximum domain size is bounded by the size of the disordered zones, which ranges from 1 to 10 nm [1,20] for typical alloys and ion irradiation conditions. Recently, it has been reported that 500 keV Ne irradiation of Cu_3Au, which forms an $L1_2$ ordered structure [23], can indeed lead to the dynamical formation of new domains in a pre-existing single domain structure; an example is illustrated in Fig. 1 [24]. The largest size of these new domains, however, exceeds 10 nm, thus beyond the largest size for disordered zones, and contrary to the model just presented.

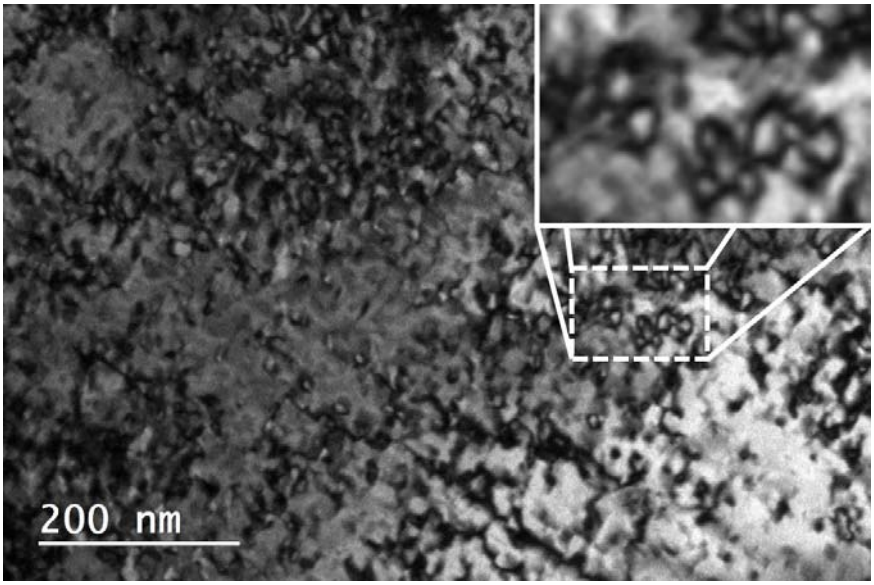

Figure 1. *Transmission electron microscopy imaging of ordered domains in $L1_2$ ordered Cu_3Au irradiated with 500 keV Ne ions at 350 ˚C at a dose rate of 1.1 10^{-4} displacement per atom per second (dpa/s) (dark field image formed using $L1_2$ superlattice reflection). Notice the presence of many, small new domain, which nucleated within the initial single domain ordered state.*

In this work, we thus investigate alternative mechanisms that could lead to patterning of order under irradiation. For that purpose we consider a model 2D binary alloy and use kinetic Monte Carlo simulations to investigate the evolution of the alloy microstructure

under irradiation, assuming that irradiation does not produce cascades, but rather is restricted to the homogeneous pairwise switching of atoms to introduce atomistic disorder, as in Eq. (1). We find that for thermodynamic parameters positioning the system close to an order-order transition, this homogeneous disordering can also stabilize patterns of order at steady state.

II. Simulations methods

1. Energetics

We consider here for simplicity a two-dimensional equiatomic alloy AB on a rigid square lattice, with pair interactions between first and second nearest neighbors. Phase equilibrium at finite temperature is determined by Ising-like interaction parameters J_s, defined for s=1, 2 by

$$J_s = \frac{1}{4}\left(2\varepsilon_{AB}^{(s)} - \varepsilon_{AA}^{(s)} - \varepsilon_{BB}^{(s)}\right) \tag{2}$$

where $\varepsilon_{ij}^{(s)}$ is the energy of an i-j pair of atoms that are "s" nearest neighbors. With this definition, alloys tend to undergo phase separation for $J_1 > 0$ and ordering for $J_1 < 0$. Owing to the competition between J_1 and J_2, however, three ground states exist for this system [25], depending on the sign and relative amplitude of J_1 and J_2, as illustrated in Fig. 2. It is convenient to introduce the ratio $R = J_2 / J_1$. For $J_1 > 0$ and $R > -½$, the ground state is analogous to a ferromagnetic state, with phase separation between pure A and pure B phases, while for $J_1 < 0$ and $R < ½$, the ground state is analogous to an antiferromagnetic state, with a 2×2 ordered structure. This is the phase investigated here,

in analogy with Cu_3Au. This ordered structure can be decomposed into two sublattices, and it possesses two variants, while the $L1_2$ ordered structure in Cu3Au has four sublattices and four variants. For $J_1 < 0$ and $R > ½$, the ground state is the so-called super-antiferromagnetic state, with a 2×1 ordered structure comprised of alternating rows of A and B atoms. The interactions considered in this study correspond to $J_1 = -0.05$ eV and R = 0.45, 0.30, 0.1 and 0. We will show that, under irradiation, the alloy system with R = 0.45, which is close to the boundary between the 2×2 and 2×1 states, behaves very differently from the others. At finite temperature, the exact nature of the equilibrium boundary between the 2×2 and 2×1 states is complex, with a non-universal behavior [26-28]. The work by Kalz et al. [29] suggests that this transition is a first order transition, with the critical temperatures of the 2×1 and 2×2 structures going to zero at the boundary. In this work, we avoid systems too close to that boundary by restricting ourselves to $R \leq 0.45$. For R = 0.45, we determine the order-disorder transition temperature for the 2×2 to 1×1 transition to be ≈ 373 K, i.e., 0.643 J_1/k_B, using the fourth-order cumulant method [30]. This value is consistent with previous reports [27,29,31], and it is significantly lower than the value for R = 0, $2/\ln(1+\sqrt{2})\ J_1/k_B \approx 2.27\ J_1/k_B$ [32], owing to the frustrations introduced by the second nearest neighbor interaction.

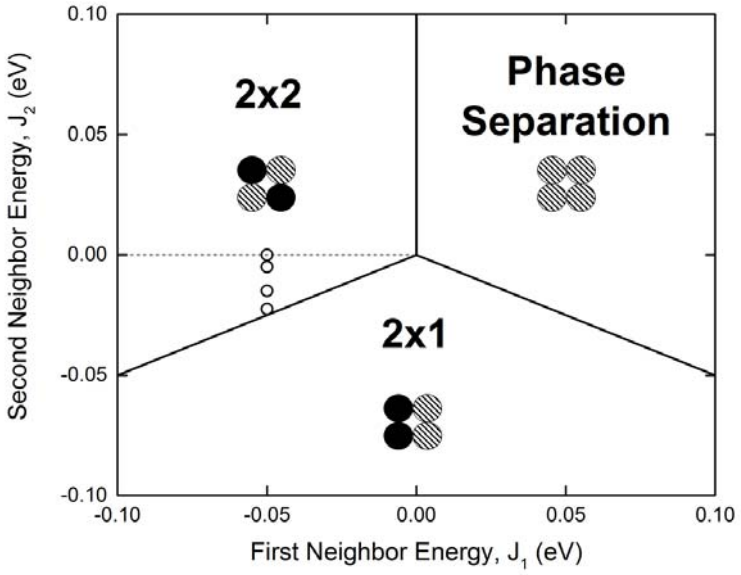

Figure 2*. Ground state diagram for the 2D square lattice with first and second nearest neighbor interactions [25]. The four small open circles correspond to the systems studied in this work.*

2. Kinetics

Two distinct kinetic processes are considered in this work. The first is thermally activated and allows the system to relax toward its equilibrium state at finite temperatures, while the second simulates the disorder introduced by energetic atomic collisions. For the thermally activated dynamics, vacancies are introduced in the 2D lattice, and atoms can migrate by exchanging positions with vacancies that are first or second nearest neighbors; second nearest neighbor jumps are included to suppress vacancy trapping on anti-site defects. For dilute vacancy concentrations, up to 2%, the kinetics is found to scale linearly with the vacancy concentration, and in the results described below, a 0.5% concentration is used to increase the efficiency of the kinetic algorithm. The jump

frequency of one such exchange between atom X, X=A, B, and a vacancy V is calculated using transition state theory

$$\Gamma_{XV} = \nu exp\left(-\frac{\Delta E_{XV}}{k_B T}\right) \tag{2}$$

where ν is an attempt frequency, set to a constant value of 10^{14} s^{-1} here for simplicity, and the activation energy is calculated using a broken bond model [33]:

$$\Delta E_{XV} = E^{sp} - \left(\sum_N^{(1)} \varepsilon_{XN}^{(1)} + \sum_M^{(2)} \varepsilon_{XM}^{(2)}\right) \tag{3}$$

where E^{sp} is a saddle point energy, assumed here to be independent of the jumping atom X, and the two summations in Eq. (3) run over the first and second shell of neighbors, respectively. The thermal jump frequencies defined by Eqs. (2,3) obey detailed balance. We restrict ourselves here to a symmetric alloy system, and without loss of generality we set $\varepsilon_{AA}^{(1)} = \varepsilon_{BB}^{(1)} = \varepsilon_{AA}^{(2)} = \varepsilon_{BB}^{(2)} = 0$ and E^{sp} = 0, as these parameters only define the absolute energy scale and the diffusion coefficient time scale, both of which are irrelevant for the present work as it focuses on determining steady states.

The second dynamic process in the model represent the atomic replacements generated by high-energy collisions [1]. As in previous works [4,34,35], these collisions are approximated by a random exchange between atoms with an imposed jump frequency Γ_b, and this process is assumed to be ballistic, i.e., athermal. The dynamics is thus equivalent to an infinite-temperature dynamics, and, when acting alone, drives the alloy into a random, disordered state. For simplicity, these exchanges are introduced one pair at a time, a situation close to high-energy electron irradiation conditions [1], between first

and second nearest neighbor sites (as for thermal jumps). This avoids, as noted above, possible complications associated with temporal and spatial correlations present in the displacement cascades created by ion and neutron irradiations [1]. .

Kinetic Monte Carlo simulations are used to obtain the evolution of the system with the thermal and the ballistic dynamics acting in parallel. As reported for similar simulations of alloys under irradiation [21,36,37], the system is observed to reach a unique steady state for any given set of T and Γ_b values, and the present work focuses on building a map of steady states in the (T, Γ_b) control-parameter space. The lattice size used in the simulations is 128×128. A residence time algorithm is employed to evolve the system in the presence of both thermal and ballistic dynamics [38,39].

3. Order state characterization

Three distinct steady states are identified by direct visualization of the alloy microstructure, namely a 1×1 disordered state, a single-domain 2×2 ordered state, and a multi-domain 2×2 ordered state. In order to identify and distinguish these three states we employ three measures of the state of chemical order present in the system. First, following Bethe [40] and Cowley [41], we define a short-range order parameter (SRO), η, based on the number of A-B bonds present in the system:

$$\eta = \frac{n_{AB} - 2zX_A X_B}{n_{AB}^{(0)} - 2zX_A X_B} \tag{4}$$

where n_{AB} and $n_{AB}^{(0)}$ are the number of A-B first nearest neighbor pairs in the current and perfectly ordered states, respectively; z is the coordination number of the first nearest neighbor shell, here 4; and X_A and X_B the A and B atomic fractions. This SRO parameter

is calculated globally, as well as locally, i.e., at every lattice site $\boldsymbol{r}_i$. Through Eq. (4) the SRO parameter is normalized so that $\eta(\mathbf{r}_j) = +1$ for perfectly ordered sites, $\eta(\mathbf{r}_j) = 0$ for disordered sites, and $\eta(\mathbf{r}_j) = -1$ for local phase separation, i.e., at anti-site defects where an atom is surrounded by 4 first nearest neighbor like-atoms. The second measure of order is a long-range order (LRO) parameter. For it, we calculate the intensity of the structure factor around a superlattice wavevector, $\boldsymbol{k}_s$,

$$I = \left\langle \left| N^{-1} \sum_j \left(\sigma_j - X_A \right) exp\left[2\pi i \left(\mathbf{k} - \mathbf{k_s} \right) \cdot \mathbf{r_j} \right] \right| \right\rangle \tag{5}$$

where N is the number of lattice sites, σ_j takes a value of 1 if the site j at $\mathbf{r}_j$ is occupied by an A atom and 0 otherwise, $\mathbf{k}_s = (1/(2a), 1/(2a))$ for the 2×2 ordered structure, a being the lattice parameter, and the brackets denote circular integration over $(\mathbf{k}-\mathbf{k}_s)$ of the structure factor, around $\mathbf{k} = \mathbf{k}_s$, up to half the Brillouin zone. This structure factor intensity is also separately calculated for a perfectly ordered lattice and for a random structure, yielding values of I_0 and I_b, respectively, so that a normalized LRO parameter S can be obtained through

$$S = \sqrt{\frac{I - I_b}{I_0 - I_b}} \tag{6}$$

The third measure of order is introduced to distinguish ordered states containing a single domain and multiple domains. For that purpose, we calculate the net "magnetization" of a configuration, M, by assigning "spin" values of +1 and -1 to atoms based on their nature and the sublattice they belong to. Specifically, decomposing the 2×2 lattice into two simple square sublattices α and β, rotated by 45° with respect to the initial

square lattice, A atoms on the α sublattice and B atoms on the β sublattice are given a +1 "spin" value, while B atoms on the α sublattice and A atoms on the β sublattice are given a -1 "spin" value. These "spin" values are then summed over the lattice and normalized by the number of atoms to obtain a net magnetization, M, varying between -1 and +1. In order to obtain a measure that is independent of the choice made in labeling the sublattices, we use $|M|$ to determine the imbalance between the two variants of the 2×2 state. Specifically, a perfectly long range ordered 2×2 state with a single domain will be characterized by $|M| \approx 1$, whereas in the case of a microstructure with multiple ordered domains resulting in similar volume fractions for the two variants of order $|M| \approx 0$. The values of η, S, and $|M|$, are essentially unaffected by the small amount of vacancies present in the simulation cell.

III. Results

We first contrast the steady states observed in the alloy system R = 0 and R = 0.45. In the case R = 0, i.e., far from the 2×2-to-2×1 boundary, at any given temperature below T_c, the system reaches a steady state with a single-domain long range ordered 2×2 state at low enough ballistic jump frequency, Γ_b. As Γ_b is increased, the LRO and SRO values at steady-state are continuously reduced, until at large enough Γ_b, the steady state becomes disordered, as illustrated in Fig. 3 for T = 0.8 T_c. This progressive disordering of the steady state is consistent with the random disorder introduced by the ballistic exchanges. In contrast, in the R = 0.45 alloy, see Fig. 4, a sequence of three steady states is observed as Γ_b is increased, starting with a single-domain long range ordered 2×2 state at low Γ_b, to a multi-domain long range ordered 2×2 state at intermediate Γ_b, to a disordered state at

high Γ_b. The multi-domain long range ordered 2×2 steady state is identified as a steady state with large values of the LRO parameter, here we imposed $S \geq 0.4$, but small values of the absolute net magnetization, here $|M| \leq 0.1$. The existence of this steady state does not correspond to any equilibrium state for this alloy, and owing to the presence of a self-selected, finite domain size, we refer to it as a state of patterning of order.

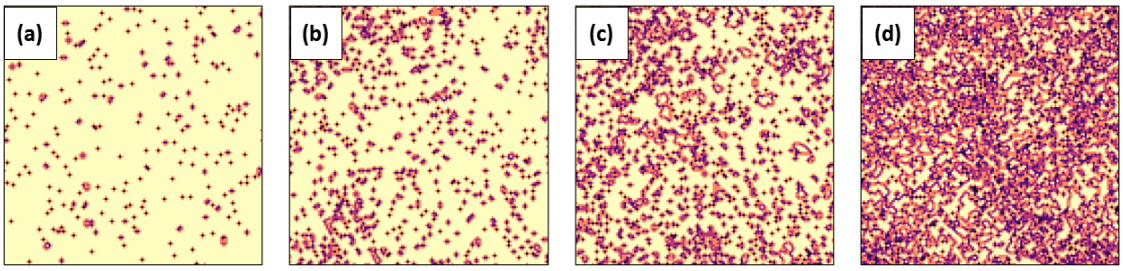

Figure 3. *Short range order η maps at steady state for the R = 0 alloy at T = 0.8 T_c and for ballistic frequency, Γ_b = 0, 6×10^7, 2×10^8, and 1×10^9 s^{-1}, from left to right. The color scale ranges from yellow (light gray) for η=1 to red (dark gray) for η=0.*

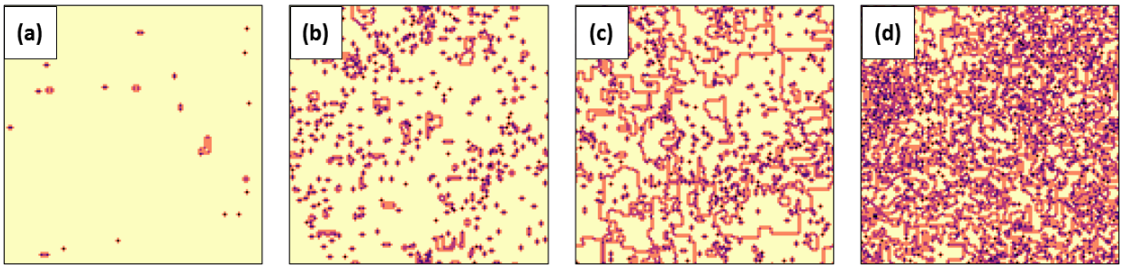

Figure 4. *Short range order η maps at steady state for the R = 0.45 alloy at T = 0.8 T_c and for ballistic frequency, Γ_b = 0, 1.2×10^3, 4.15×10^3, and 3×10^4 s^{-1}, from left to right. The color scale ranges from yellow (light gray) for η=1 to red (dark gray) for η=0.*

Two additional points are worth noticing regarding the multi-domain steady state. First, the microstructure of the alloy in this state contains many ordered domains, and larger domains often contain several embedded, smaller domains of the opposite variant. Direct visualization of the temporal evolution of the system shows that this domain structure is a dynamical one, continuously evolving. In particular, some domains coarsen, but with new domains nucleating within these larger domains, preventing the system

from reaching a single-domain steady state. These new domains nucleate by the migration and aggregation of anti-sites that are randomly introduced by ballistic exchanges. In the R = 0.45 alloy, the nucleation rate is high, as suggested from Fig. 4, while new domains are rarely observed in the R = 0 alloy, see Fig. 3. The second point is that for the R = 0.45 alloy the domain (or anti-phase boundaries, APBs) tend to be faceted along the <10> directions, suggesting that the excess energy of these APBs is low in this alloy. These two points are in fact related, as will be discussed in Section IV.

In order to determine possible influences of the initial state on the steady state microstructure, for all parameter reported here, simulations were initiated with two opposite states of order, a single-domain perfectly ordered 2×2 state and a fully random, disordered state. For these two initial states, the systems always reach the same steady state values of order parameters η and S, as illustrated in Fig. 5 for the alloy R = 0.45, T = 0.8 T_c and $\Gamma_b = 3 \times 10^3$ s^{-1}. This invariance of the steady state indicates that the dissipative systems studied here are ergodic. We used this property to determine when systems had reached their steady state for building the steady-state maps presented below.

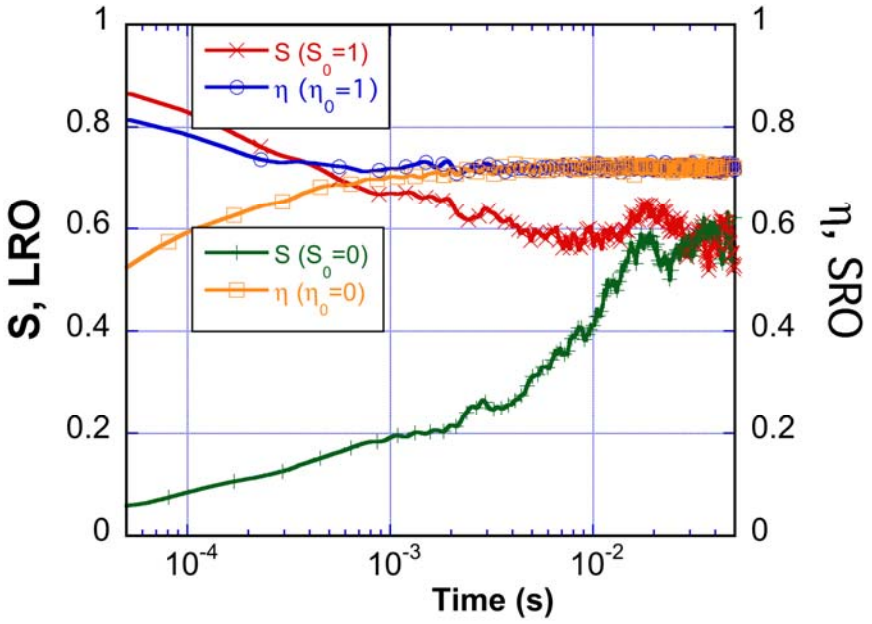

***Figure** 5. Temporal evolution of the short-range order (SRO) parameter η and the long range order (LRO) parameter S for R = 0.45 alloy, T = 0.8 T_c and $\Gamma_b = 3 \times 10^3\ s^{-1}$. Systems initially ordered and initially disordered reached the same steady state. As expected, the SRO reaches steady state at shorter times than the LRO, and fluctuations are larger for the LRO evolution than for the SRO one.*

The overall evolution of these driven alloys can be captured by building steady-state maps of η, S, and $|M|$ in the (T, Γ_b) control parameter space, as seen in Fig. 6 for R = 0 and Fig. 7 for R = 0.45.

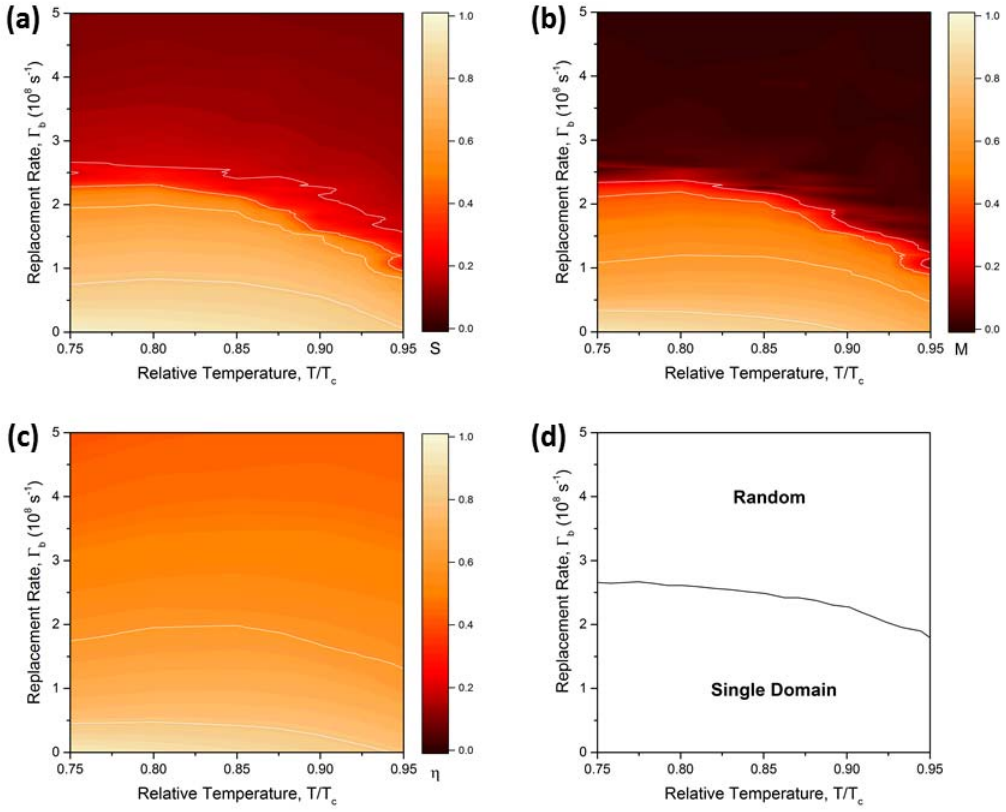

Figure 6. *For alloy R = 0, steady state values of (a) long range order parameter, S; (b) absolute net magnetization, |M|; and (c) short range order parameter, η, as function of temperature and replacement rate* Γ_b. *Initial condition is fully ordered 2x2 state. Maps are constructed from 540 (T,* Γ_b*) points. White contour lines are added to highlight 20% decreases in the parameters. Overall phase diagram is displayed in (d) using criteria given in text.*

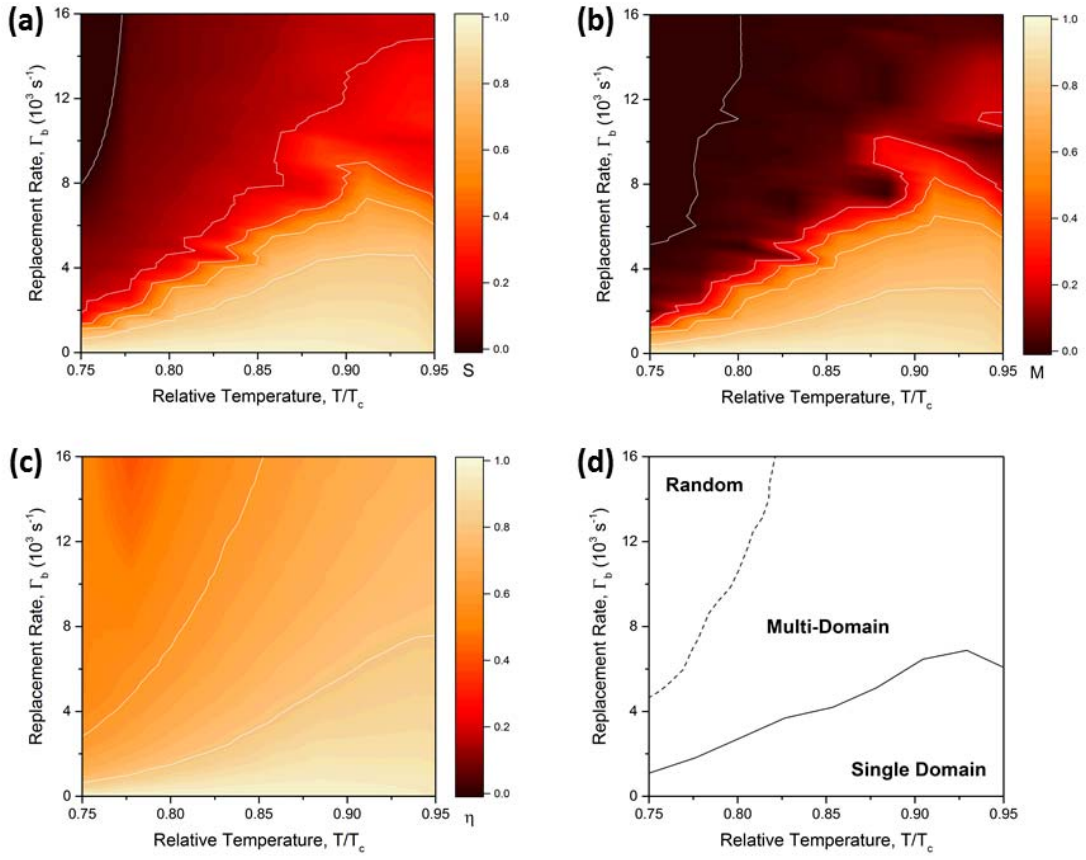

Figure 7*. For alloy R = 0.45, steady state values of (a) long range order parameter, S; (b) absolute net magnetization, |M|; and (c) short range order parameter, η, as function of temperature and replacement rate* Γ_b*. Initial condition is fully ordered 2x2 state. Maps are constructed from 340 (T,* Γ_b*) points. White contour lines are added to highlight 20% decreases in the parameters. Overall phase diagram is displayed in (d) using criteria given in text.*

The most notable result of Figs. 6 and 7 is the existence of a region in the (T, Γ_b) space where the alloy with R = 0.45 stabilizes into a multi-domain long-range ordered 2×2 steady state. This domain, moreover, exists for a broad range of ballistic jump frequencies, especially as the temperature approaches T_c. The transition from the multi-domain state to the disordered state is more difficult to locate, as the domain size is

gradually reduced when Γ_b is increased. This transition is estimated here using a threshold value for the long-range order parameter of $S_{th} = 0.1$. This choice is based on observations that the equilibrium value of S drops below 0.1 for T above $\approx 1.2\ T_c$. More accurate determinations are possible, for instance by deconvolving the superlattice intensity into SRO and LRO contributions [22], but the present criterion is sufficient for establishing the existence of the patterning of order, and determining the mechanisms responsible for its stabilization.

The non-equilibrium phase diagrams in Figs. (6,7) were calculated in the (T, Γ_b) control-parameter space. For dissipative systems at steady state, it is however physically insightful to evaluate the forcing conditions by using a reduced forcing intensity γ [4]. In systems described by Eq. (1), for instance, the driven steady state is equivalent to the thermodynamic equilibrium state of an effective alloy described by the effective free energy $F_{eff} = F + \gamma S^2/2$, with $\gamma = \Gamma_b / M$. In the present KMC simulations, the forcing intensity is directly obtained by measuring the ratio of ballistic jumps to vacancy jumps [36]. It is interesting in particular to determine this forcing intensity near the transition between different steady states. For the R = 0 alloy, at T = 0.8 T_c for instance, the transition between ordered to disordered steady states occurs for $\Gamma_b \approx 2.6 \times 10^8\ s^{-1}$, and the corresponding forcing intensity is measured to be 5.0×10^{-2}. This forcing intensity is similar to values reported for other order-disorder transitions driven by ballistic exchanges [36]. In contrast, in the R = 0.45 alloy, the forcing intensity at the transition between the single-domain to the multiple-domain steady state is significantly lower. For T = 0.8 T_c, this transition takes place for $\Gamma_b \approx 3 \times 10^3\ s^{-1}$, resulting in a forcing intensity

of $\approx 5.2 \times 10^{-3}$. The fact that such a low forcing intensity is sufficient to destabilize a long-range ordered state to the benefit of a patterning of order steady state adds further support to our previous observation that, in the R = 0.45 alloy, the disorder introduced by ballistic exchanges couples very strongly with thermally activated relaxation processes, in particular those controlling nucleation of new domains and APB migration. This point is further discussed in the next section.

IV. Discussion

The primary result of this work is that the atomic-scale disorder introduced by isolated ballistic events can stabilize a steady state microstructure where multiple long-range ordered domains dynamically coexist. In contrast to past studies where the ballistic events were introduced in the form of large disordered zones, which could promote directly the nucleation of new domains, the present work introduces ballistic events one pair of antisites at a time. All prior simulations using this latter irradiation condition concluded that below T_c the system should stabilize into a single-domain long-range ordered state at low ballistic jump frequency and a disordered state at high ballistic jump frequency [21,22,36,42]. These past results are in fact in good agreement with the present simulations when the ratio of first to second nearest neighbor interactions, *R*, is such that the system is well inside the stability region of the 2×2 "antiferromagnetic" ordered state, i.e., $R = 0$ to $R = 0.3$. Patterning of order is observed, on the other hand, when *R* is such that the alloy is close to the boundary between the 2×2 ordered state and the 2×1 "super-antiferromagnetic" ordered state, e.g., $R = 0.45$. Analysis of the system microstructure

and evolutions reveals that in this alloy antisite migration can lead to their clustering and to the formation of new, anti-phase domains. Furthermore, antiphase domain boundaries (APBs) are faceted along the <10> directions.

A first rationalization of these results can be obtained by analyzing the energetics of a perfectly ordered 2×2 state containing a few antisites. Simple bond counting indicates that the excess energy of one A_β antisite, i.e., an A atom occupying a β sublattice site, is given by $\Delta E_{AS}^{(1)} = 4\left(\varepsilon_{AA}^{(1)} - \varepsilon_{AB}^{(1)}\right) + 4\left(\varepsilon_{AB}^{(2)} - \varepsilon_{BB}^{(2)}\right)$, see Fig. 8(a). For alloys with symmetric interaction parameters as considered here, the excess energy is the same for A_β and B_α antisites, so it can be directly expressed in terms of the coupling constants J_1 and J_2 as $\Delta E_{AS}^{(1)} = -8J_1 + 8J_2 = -8J_1(1-R)$. Turning then to one pair of antisites, one finds that two second-nearest neighbor A_β antisites repel each other for $R \geq 0$. Opposite antisites A_β and B_α, in contrast, can form stable first nearest neighbor pairs, as the excess energy per antisite of one such pair is calculated to be $\Delta E_{AS}^{(2)} = -6J_1 + 8J_2 = -6J_1(1-4R/3)$, which is always less than $\Delta E_{AS}^{(1)}$. More generally, in the case of n first nearest neighbor antisites ($n \geq 1$) aligned along a <10> direction, the excess energy per antisite becomes $\Delta E_{AS}^{(n)} = -4\frac{n+1}{n}J_1(1-\frac{2n}{n+1}R)$. The excess energy per antisite therefore decreases as n increases, and in the limit $n \to \infty$, it reaches the limit $\Delta E_{AS}^{(\infty)} = -4J_1(1-2R)$. The remarkable result is that this excess energy goes to zero at R = ½. As R approaches ½, there is thus a strong energetic bias for pairs of opposite antisites A_β-B_α to form bound pairs. Opposite antisites could also recombine, of course, but this recombination requires a sequence of correlated vacancy jumps. It is thus also

expected for R approaching ½ that the rate of formation and the stability of bound pairs greatly increase as the concentration of antisites increases, i.e., as the ballistic jump frequency Γ_b increases.

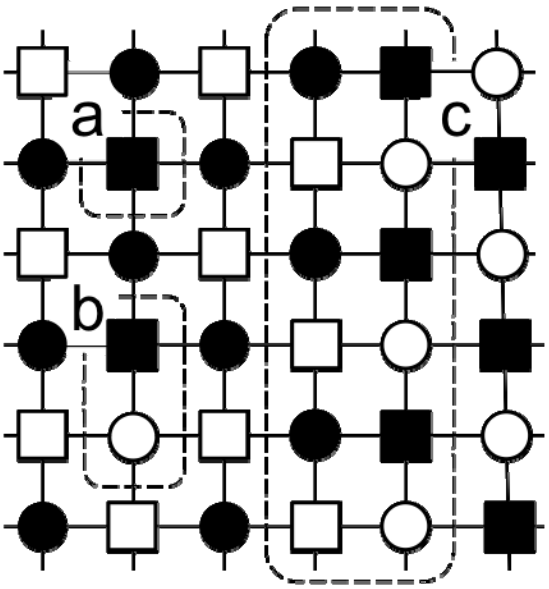

***Figure 8**: Various configurations of antisites and disorder on the 2×2 square lattice, here decomposed into α and β sublattice sites, represented by circles and squares, respectively, with A atoms and B atoms shown as black and white symbols, respectively. (a) isolated A_β antisite; (b) pair of first nearest neighbor A_β-B_α antisites; and (c) (10) antiphase boundary.*

It is also interesting to relate the excess energy of bound antisites to the excess energy of antiphase boundaries. As illustrated in Fig. 8(c), it is readily seen that the excess energy per unit length a of an infinite {10} APB is directly related to $\Delta E_{AS}^{(\infty)}$ through $\gamma_{APB}^{\{10\}} = \Delta E_{AS}^{(\infty)} / (2a) = -2J_1(1-2R)/a$. The presence of low-energy APBs as R approaches ½ is thus fully consistent with the {10} faceting of APBs observed in the simulations, see for instance Fig. 4(c,d). We also note that atoms in the core of these APBs are organized in motifs that are embryos of the 2×1, "super-antiferromagnetic" state. The fact that $\gamma_{APB}^{(10)} \to 0$ as $R \to$ ½ is thus directly related to the degeneracy of the

ground state between the 2×1 and 2×2 ordered structures for R = ½. The net conclusion of this discussion is that a simple consideration of the energetics of antisite interactions provides a reasonable rationalization for the observations reported in Section III that, for R = 0.45, antisites can cluster and form nuclei for antiphase domains.

We next illustrate how the kinetic stabilization of bound antisites can lead to the patterning of order. For this purpose we modify a model previously introduced to account for patterning of order under irradiation conditions that result in the formation of disordered zones by displacement cascades [43]. The model relies on the idea that in the patterning state there is an equal volume fraction of the antiphase domains allowed by the symmetry of the ordered phase, whereas in a single-domain LRO state, the microstructure contains only one macroscopic variant. The transition from one steady state to another can thus be captured by monitoring the area fraction occupied by one variant, A_1. This evolution is coupled to that of the APB length per unit area, L_{APB}, and to the concentration of antisites. We derive in Appendix A, the defining equations for how irradiated system will evolve and provide steady-state solutions. The key results are: At low ballistic jump frequency, $A_1 = ½$ is an unstable solution, just as it is in the absence of irradiation. The order microstructure is thus expected to coarsen in such a way that one ordered domain, say belonging to variant 1, overruns the whole volume, i.e., $A_1 \to 1$. At higher ballistic jump frequency, however, $A_1 = ½$ becomes a stable solution, and the APB length per unit area stabilizes at a non-zero value. This solution thus corresponds to the patterning of order steady state. While the above model is phenomenological, it provides direct support for the conclusion reached earlier that the clustering of antisites and the ensuing nucleation of new domains, as observed in the simulations, are processes that can

stabilize patterns of order. Returning to Eq. (1), it suggests that the patterning observed here results from a coupling between the dissipation of the excess free energy due to nonequilibrium antisites and the domain boundary dynamics, a coupling that cannot be captured by Eq. (1) in its present form. One possible path to address this limitation would be to replace the scalar order parameter S by a two-dimensional order parameter that would describe the 2×2 and the 2×1 structures at once, since APBs of the 2×2 structure can be seen as very small elements with a 2×1 ordered state, and to take into account that thermally activated jumps are mediated by vacancies. This extended model would capture key thermodynamic and kinetic couplings between the disorder introduced by irradiation and the relaxation rates of this two-dimensional order parameter, and, as such, it might be able to generate patterning of order at steady state.

The results presented in this work focused on a simple 2D model alloy near a degenerate state. The analysis of these results indicate that ordering frustrations near this degenerate state biased the energy dissipation of the disorder introduced by ballistic jumps, leading to the kinetic stabilization of APBs and to patterning of order. This suggests that patterning of order under irradiation could be found in more complex alloy systems where the above requirements are met. The present results also indicate that, unlike the compositional patterning induced by finite-range mixing [6] and the order patterning induced by disordered zones [21,22], this novel patterning reaction does not rely on a finite length scale introduced by the external forcing. The possibility of irradiation-induced patterning without such an external length scale has been established for phase separating systems [44,45] but, to our knowledge, this is the first time that it is proposed by systems undergoing chemical ordering.

In the context of the recent findings of spontaneous domain formation in $L1_2$ ordered Cu_3Au alloys during Ne ion irradiations [24] shown in Fig. 1, it is interesting to consider whether the above requirements could be met in Cu_3Au. We first note that {100} APBs in Cu_3Au exhibit strong faceting at equilibrium, thus suggesting that these APBs carry very low excess free energy. While it is problematic to calculate APB energies from standard first principles techniques [46,47] in Cu_3Au, mean-field models provide simple expressions for the energy of an $L1_2$ ordered state and its APBs as linear combination of the pairwise interaction parameters J_1, J_2, J_3 [48]. It is commonly assumed (and observed) that the strength of these pairwise interactions decrease with the interaction range, so that J_1 should play a dominant role. Remarkably, J_1 is absent from the expression of {100} APBs, thus providing further support to the idea that {100} APBs carry low excess energy. Lastly, for $J_1 < 0$, the ground state is degenerate between the $L1_2$ and $D0_{22}$ ordered structures for $J_2 = 0$ [23]. The energetics of an $L1_2$ alloy with $|J_2| \gg |J_1|$ therefore shares key characteristics with the 2D square lattice model considered here when R approaches ½. It thus appears possible that under irradiation stable antisite clusters would form, and then contribute to the nucleation of new ordered domains, as observed in Fig. 1.

Further work is needed, however, to test this hypothesis for Cu_3Au, especially since nonequilibrium point defects play an important role in ordering and disordering kinetics under irradiation [49]. In the present model, the description of point defects has been simplified by ignoring interstitials and by treating vacancies as a conserved species. Additional simplifications were made in the parametrization of the kinetic model, including allowing vacancies to jump to first and second nearest neighbor sites to avoid vacancy trapping and using symmetric energy interaction parameters. Since these settings

affect the dependence of the thermal mobility, M_o in Eq. (1), with the local order parameters, they can modify the steady state reached by the system, as well as the transitions from one steady state to another. Overall, a predictive kinetic model for Cu_3Au under irradiation should therefore not only be based on the $L1_2$ ordered structure, but include realistic treatment of point defect creation, migration, recombination and annihilation on sinks [50-52], along with a fuller account of irradiation-induced chemical disorder in nuclear collisions, as done for instance in ref. [8].

V. Conclusion

Kinetic Monte Carlo simulations were employed to investigate the effect of ballistic disordering on the order microstructure of a 2D binary alloy on a square lattice, with first and second nearest neighbor interactions chosen to stabilize a 2×2 ordered structure at thermodynamic equilibrium. When the ratio R of second to first interaction energies approaches ½, a value where a degenerate state would exist at 0 K in the absence of ballistic jumps, it is observed that three possible steady states exist in the presence of ballistic jumps, namely disordered, long-range ordered with a single domain, or long-range ordered with multiple domains that coexist dynamically. The stabilization of this third steady state, which corresponds to a self-organization of the driven alloy into patterns of order, is discussed by considering the dynamics of antisites and APBs under irradiation. In the R = 0.45 alloy, it is shown that pairs of antisites can form stable bound complexes, which then serve as nuclei for the formation of antiphase domains embedded in larger domains. From this analysis, it is proposed that this novel mechanism of patterning of order under irradiation can take place in more complex alloy systems,

including Cu_3Au, for which recent experiments suggest that ion irradiation can lead to the continuous formation of antiphase domains.

Acknowledgement

This work was supported by the U.S. Department of Energy, Office of Science, Basic Energy Sciences, under Award # DE-FG02-05ER46217. We thank Dr. Thomas Garnier (ROBATEL Industries, Lyon, France) for helpful discussions.

Appendix A. Phenomenological model for patterning of order under irradiation

We detail here a simple model to capture the transition from a single-domain long range ordered state to a state of patterning of order where multiple ordered domains coexist. Following the derivation in ref. [43] for an ordered state with 2 variants, the evolution of the APB length per unit area, L_{APB}, and of the variant area fraction, A_1, in the absence of irradiation, can be written as:

$$\frac{dL_{APB}}{dt} = -g_1 M_{APB} \left(L_{APB} \right)^3 \tag{A1a}$$

$$\frac{dA_1}{dt} = -g_2 M_{APB} \left(L_{APB} \right)^2 \left(\frac{1}{2} - A_1 \right) \tag{A1b}$$

where M_{APB} is a mobility of antiphase boundaries, and g_1 and g_2 geometric factors. The first equation is the standard Allen-Cahn equation [15]. The second equation indicates that $A_1 = ½$ is an unstable steady state under thermal annealing, consistent with the fact that one variant should progressively invade the whole microstructure in this case. As

discussed in Section IV, the key irradiation effect for patterning is the formation of bound pairs of antisite. By analogy with rate equation models for point defects under irradiation [53], we introduce a simple rate equation to describe the evolution of the site fraction of antisites, C_{anti},

$$\frac{dC_{anti}}{dt} = \frac{1}{2}\Gamma_b - K_r C_{anti}^{\ 2} - K_b C_{anti}^{\ 2} \tag{A2a}$$

where K_r and K_b are rate constants for recombination and for the formation of bound pairs, respectively. In the above equation, the absorption of antisites by APBs has been neglected for simplicity. The formation of bound pairs of antisites leads to the creation of new APBs and new domains, and paralleling again the derivations from ref. [43], these effects can be captured by modifying Eqs. (A1a,b)

$$\frac{dL_{APB}}{dt} = -g_1 M_{APB}\left(L_{APB}\right)^3 + \ell K_b C_{anti}^2 \tag{A3a}$$

$$\frac{dA_1}{dt} = -g_2 M_{APB}\left(L_{APB}\right)^2\left(\frac{1}{2} - A_1\right) + 2\mathcal{A}K_b C_{anti}^2\left(\frac{1}{2} - A_1\right) \tag{A3b}$$

where ℓ and $\mathcal{A}$ are respectively the APB length per unit area and the specific domain area, generated by the clustering of pairs of antisites. We set the irradiation term in Eq. (A3b) proportional to $(1/2\text{-}A_1)$ since the generation rate of new domains, e.g., of variant 1, increases as the overall fraction of the variant 2 increases. As the coefficient for this term is positive, it tends to stabilize microstructures with $A_1 = A_2 = ½$.

The evolution of the domain area fraction is the main point of interest here, and in the case of patterning of order it is expected that at steady state $A_1 = ½$ be a stable solution, whereas in the case of a single-domain 2×2 ordered state, A_1 should evolve

toward 0 or 1. We thus focus now on the stability of the $A_1 = ½$ solution in Eq. (A3b). This stability is determined by the relative magnitude of the coefficients for the first and second terms in the right-hand side of Eq. (A3b) since these two terms are linear in (½ - A_1). These two coefficients are however functions of C_{anti} and L_{APB} and so, in principle, one would need to solve for the coupled evolution of the three Eqs. (A2, A3a, A3b). A first simplification is obtained by performing an adiabatic elimination of C_{anti}, using its steady state value in Eqs. (A3a, A3b), since the antisite population reaches its steady state much faster than L_{APB} and A_1. Second, Eq. (A3a) yields a unique, stable steady state for L_{APB}, which is finite and positive for finite ballistic jump frequency Γ_b. In order to assess the competition between the two terms in the domain area equation, Eq. (A3b), it is thus sufficient to replace the time-dependent L_{APB} by its steady state value, yielding

$$\frac{dA_1}{dt} = -\left[g_2 M_{APB} \left(\frac{\ell}{2g_1} \frac{K_b}{K_b + K_r} \frac{\Gamma_b}{M} \right)^{2/3} - \mathcal{A} \frac{K_b}{K_b + K_r} \Gamma_b \right] \left(\frac{1}{2} - A_1 \right) = \lambda \left(\frac{1}{2} - A_1 \right) \quad \text{(A4)}$$

Analysis of the two terms in the bracket of the right-hand side in Eq. (A4) indicates that, at low ballistic jump frequency Γ_b, the first term dominates, so that λ is positive, and $A_1 = ½$ is an unstable steady state, i.e., the system forms a single domain 2×2 ordered state. As Γ_b increases, there is a critical value where λ changes sign and becomes negative, thus transforming the $A_1 = ½$ into a stable steady state, i.e., stabilizing a multi-domain 2×2 ordered state. This simple analysis assumes that Γ_b is small enough for the alloy to remain long range ordered over this whole range. While the above continuum model could be improved in many ways, it captures the transition from single-domain to multi-domain 2×2 ordered states and provides a simple physical picture for some of the

parameters controlling this transition. In the case of an alloy system where the rate of formation of bound pairs of antisites is negligible compared to the antisite recombination rate, e.g., R = 0, 0.1 and 0.3, the ratio $K_b/(K_b + K_r)$ become negligible, and L_{APB} and A_1 evolve then similarly to equilibrium systems, with a single-domain 2×2 ordered state, until Γ_b is so large that the steady state transitions to a disordered state.

References

[1] R. S. Averback and T. D. de la Rubia, Displacement damage in irradiated metals and semiconductors, Solid State Physics, Vol 51 **51**, 281 (1998).
[2] G. Martin and P. Bellon, Driven alloys, Solid State Phys **50**, 189 (1997).
[3] P. Sigmund, *Particle Penetration and Radiation Effects* (Springer Verlag, Berlin-Heidelberg, Germany, 2006), Solid State Sciences.
[4] G. Martin, Phase-Stability under Irradiation - Ballistic Effects, Phys Rev B **30**, 1424 (1984).
[5] M. C. Cross and P. C. Hohenberg, Pattern-Formation Outside of Equilibrium, Rev Mod Phys **65**, 851 (1993).
[6] R. A. Enrique and P. Bellon, Compositional patterning in systems driven by competing dynamics of different length scale, Phys Rev Lett **84**, 2885 (2000).
[7] R. A. Enrique and P. Bellon, Compositional patterning in immiscible alloys driven by irradiation, Phys Rev B **63**, 134111 (2001).
[8] R. A. Enrique, K. Nordlund, R. S. Averback, and P. Bellon, Simulations of dynamical stabilization of Ag-Cu nanocomposites by ion-beam processing, J Appl Phys **93**, 2917 (2003).
[9] G. Demange, L. Luneville, V. Pontikis, and D. Simeone, Prediction of irradiation induced microstructures using a multiscale method coupling atomistic and phase field modeling: Application to the AgCu model alloy, J Appl Phys **121**, 125108 (2017).
[10] R. A. Enrique and P. Bellon, Self-organized Cu-Ag nanocomposites synthesized by intermediate temperature ion-beam mixing, Appl Phys Lett **78**, 4178 (2001).
[11] P. Krasnochtchekov, R. S. Averback, and P. Bellon, Phase separation and dynamic patterning in Cu1-xCox films under ion irradiation, Phys Rev B **72**, 174102 (2005).
[12] S. W. Chee, B. Stumphy, N. Q. Vo, R. S. Averback, and P. Bellon, Dynamic self-organization in Cu alloys under ion irradiation, Acta Mater **58**, 4088 (2010).
[13] B. Stumphy, S. W. Chee, N. Q. Vo, R. S. Averback, P. Bellon, and M. Ghafari, Irradiation-induced patterning in dilute Cu-Fe alloys, J Nucl Mater **453**, 66 (2014).
[14] P. C. Hohenberg and B. I. Halperin, Theory of Dynamic Critical Phenomena, Rev Mod Phys **49**, 435 (1977).
[15] S. M. Allen and J. W. Cahn, A microscopic theory for antiphase boundary motion and its application to antiphase domain coarsening, Acta Metallurgica **27**, 1085 (1979).
[16] L. R. Aronin, Radiation Damage Effects on Order-Disorder in Nickel-Manganese Alloys, J Appl Phys **25**, 344 (1954).
[17] E. M. Schulson, The ordering and disordering of solid solutions under irradiation, J Nucl Mater **83**, 239 (1979).

[18] J. W. Liu and P. Bellon, Patterning and ordering in driven alloys with coupled conserved and nonconserved order parameters, Phys Rev B **66**, 020303 (2002).
[19] M. L. Jenkins, K. H. Katerbau, and M. Wilkens, Transmission Electron-Microscopy Studies of Displacement Cascades in Cu3au .1. Diffraction Contrast of Disordered Zones, Philos Mag **34**, 1141 (1976).
[20] M. L. Jenkins and M. Wilkens, Transmission Electron-Microscopy Studies of Displacement Cascades in Cu3au .2. Experimental Investigation of Cascades Produced by Energetic Cu+ Ions, Philos Mag **34**, 1155 (1976).
[21] J. Ye and P. Bellon, Nanoscale patterning of chemical order induced by displacement cascades in irradiated alloys. I. A kinetic Monte Carlo study, Phys Rev B **70**, 094104 (2004).
[22] J. Ye and P. Bellon, Nanoscale patterning of chemical order induced by displacement cascades in irradiated L1(0) alloys: Scaling analysis of the fluctuations of order, Phys Rev B **73**, 224121 (2006).
[23] F. Ducastelle, *Order and phase stability in alloys* (North-Holland ; Elsevier Science Pub. Co., Amsterdam ; New York, NY, USA, 1991).
[24] C. R. Lear, PhD thesis, http://hdl.handle.net/2142/95309, University of Illinois at Urbana-Champaign, 2016.
[25] C. Fan and F. Y. Wu, Ising Model with Second-Neighbor Interaction .I. Some Exact Results and an Approximate Solution, Phys Rev **179**, 560 (1969).
[26] K. Tanaka, T. Horiguchi, and T. Morita, Critical Indexes for the 2-Dimensional Ising-Model with Nearest-Neighbor and Next-Nearest-Neighbor Interactions .2. Strip Cluster Approximation, Physica A **192**, 647 (1993).
[27] K. Binder and D. P. Landau, Phase-Diagrams and Critical-Behavior in Ising Square Lattices with Nearest-Neighbor and Next-Nearest-Neighbor Interactions, Phys Rev B **21**, 1941 (1980).
[28] S. Ranjbar, The Exact Determination of the Critical Points for 2-D Square Lattice Ising Model with the Nearest and Next Nearest Neighbors Interactions, J Iran Chem Soc **8**, 872 (2011).
[29] A. Kalz, A. Honecker, S. Fuchs, and T. Pruschke, Monte Carlo studies of the Ising square lattice with competing interactions, J Phys Conf Ser **145**, 012051 (2009).
[30] K. Binder, Phase-Transitions in Reduced Geometry, Annu Rev Phys Chem **43**, 33 (1992).
[31] J. Oitmaa, The Square-Lattice Ising-Model with 1st and 2nd Neighbor Interactions, J Phys a-Math Gen **14**, 1159 (1981).
[32] L. Onsager, Crystal statistics I A two-dimensional model with an order-disorder transition, Phys Rev **65**, 117 (1944).
[33] G. Martin, Atomic Mobility in Cahn Diffusion-Model, Phys Rev B **41**, 2279 (1990).
[34] R. A. Enrique and P. Bellon, Phase stability under irradiation in alloys with a positive heat of mixing: Effective thermodynamics description, Phys Rev B **60**, 14649 (1999).
[35] F. Soisson, P. Bellon, G. Martin, and E. Salomons, Interphase and Antiphase Boundary Stability in Bcc Compounds under Irradiation, J Nucl Mater **205**, 324 (1993).
[36] E. Salomons, P. Bellon, F. Soisson, and G. Martin, Dynamic Lattice Models for Binary-Alloys under Irradiation - Mean-Field Solutions and Monte-Carlo Simulations, Phys Rev B **45**, 4582 (1992).
[37] S. P. Shu, P. Bellon, and R. S. Averback, Complex nanoprecipitate structures induced by irradiation in immiscible alloy systems, Phys Rev B **87** 144102 (2013).
[38] A. B. Bortz, M. H. Kalos, and J. L. Lebowitz, New Algorithm for Monte-Carlo Simulation of Ising Spin Systems, J Comput Phys **17**, 10 (1975).
[39] T. A. Abinandanan, F. Haider, and G. Martin, Monte-Carlo Simulations of Precipitation of L1(2) Ordered Phase, Proceedings of an International Conference on Solid - Solid Phase Transformations, 443 (1994).

[40] H. A. Bethe, Statistical theory of superlattices, Proceedings of the Royal Society A: Mathematical, Physical and Engineering Sciences **150**, 552 (1935).
[41] J. M. Cowley, An Approximate Theory of Order in Alloys, Phys Rev **77**, 669 (1950).
[42] F. Soisson, P. Bellon, and G. Martin, 2-Phase Dynamic Equilibria Driven by Irradiation in Ordered Alloys, Phys Rev B **46**, 11332 (1992).
[43] J. Ye and P. Bellon, Nanoscale patterning of chemical order induced by displacement cascades in irradiated alloys. II. Analytical modeling, Phys Rev B **70**, 094105 (2004).
[44] G. Martin, Contribution of Dissipative Processes to Radiation-Induced Solid-Solution Instability, Phys Rev B **21**, 2122 (1980).
[45] G. Martin, Long-Range Periodic Decomposition of Irradiated Solid-Solutions, Phys Rev Lett **50**, 250 (1983).
[46] Y. S. Zhang, G. Kresse, and C. Wolverton, Nonlocal First-Principles Calculations in Cu-Au and Other Intermetallic Alloys, Phys Rev Lett **112**, 075502 (2014).
[47] L. Y. Tian, H. Levamaki, M. Ropo, K. Kokko, A. Nagy, and L. Vitos, Exchange-Correlation Catastrophe in Cu-Au: A Challenge for Semilocal Density Functional Approximations, Phys Rev Lett **117**, 066401 (2016).
[48] O. I. Gorbatov, I. L. Lomaev, Y. N. Gornostyrev, A. V. Ruban, D. Furrer, V. Venkatesh, D. L. Novikov, and S. F. Burlatsky, Effect of composition on antiphase boundary energy in Ni3Al based alloys: Ab initio calculations, Phys Rev B **93**, 224106 (2016).
[49] L. Wei, Y. S. Lee, R. S. Averback, and C. P. Flynn, Antistructure and point defect response in the recovery of ion-irradiated Cu(3)An, Phys Rev Lett **84**, 6046 (2000).
[50] S. P. Shu, P. Bellon, and R. S. Averback, Role of point-defect sinks on irradiation-induced compositional patterning in model binary alloys, Phys Rev B **91**, 214107 (2015).
[51] F. Soisson, Kinetic Monte Carlo simulations of radiation induced segregation and precipitation, J Nucl Mater **349**, 235 (2006).
[52] F. Soisson and T. Jourdan, Radiation-accelerated precipitation in Fe-Cr alloys, Acta Mater **103**, 870 (2016).
[53] R. Sizmann, The Effect of Radiation Upon Diffusion in Metals, J Nucl Mater **69 & 70**, 386 (1978).